Active control of a non-smooth nonlinear system using feedback linearisation

Domenico Lisitano[1], Shakir Jiffri[2], Elvio Bonisoli[3] and John E Mottershead[4]

[1,3]*Dipartimento di Produzione, Politecnico di Torino, Corso Duca degli Abruzzi, 24, 10129 Torino, Italy*

[2,4]*Centre for Engineering Dynamics, University of Liverpool, Liverpool L69 3GH, UK*

ABSTRACT

Partial feedback linearisation is applied to an experimental nonlinear non-smooth mechanical system with three degrees of freedom and opening and closing gaps to produce a piecewise-linear stiffness characteristic. Stepped sine testing shows that the second mode is strongly affected by the nonlinearity whereas the first and third modes remain essentially linear. A mathematical model is tuned to accurately reproduce the nonlinear test behaviour, including jump phenomena. The classical theory of feedback linearisation is then briefly reviewed and feedback gains are determined based on the tuned model with the purpose of pole assignment. The zero dynamics are found to be stable. Closed-loop tests are carried out to assign linear viscous damping ratios to the linearised system. These are measured using the logarithmic decrement and found to be in very good agreement with demanded values.

Keywords: *Active control, feedback linearisation, non-smooth nonlinear system, piecewise linearity*

1 INTRODUCTION

In the recent past, the research problems have increasingly been targeted toward nonlinear systems, to meet the growing need to improve performance and reducing weight and volume of mechanical components. While the control theory of linear systems is well developed, the nonlinear one attempts to extend these methods to be applicable to more general, found in many real-life, practical situations. This paper deals with the application of feedback linearisation to non-smooth nonlinear systems. The feedback linearisation method is clearly presented in many well-known texts [1-3]. Essentially, the method allows one to transform a nonlinear system to an equivalent linear one, through appropriate choice of input. Complete input-output feedback linearisation results in the linearisation of all the outputs of a plant [4-5]; the partial version is a particular approach to apply the feedback linearization, it consists of linearising only some of the outputs of a plant: robots [6-8], overhead cranes [9-10], induction motors [11] and pneumatic actuators [12] controls are only some examples, but all of them refer to smooth nonlinearities. Much less has been done with non-smooth nonlinear systems, perhaps because one of the original requirements for the application of feedback linearisation is the smoothness of the nonlinear behaviour. This constraint has been proven to be unnecessary at least in cases where the nonlinearity has a dead zone, piecewise, backlash or hysteresis characteristics in the input [13-14] and in [15] the theory of

[1] domenico.lisitano@polito.it*

[2] S.Jiffri@liverpool.ac.uk

[3] elvio.bonisoli@polito.it

[4] J.E.Mottershead@liverpool.ac.uk

* Corresponding author

complete and partial feedback linearisation is developed for systems with structural non-smooth nonlinearity.

In this paper, partial feedback linearisation is applied to a non-smooth, nonlinear simple three degree-of-freedom mass-spring system. The experimental rig is accompanied by a representative numerical model, which is used for simulation purposes and also for real-time control. In the §2, the design of the three degree-of-freedom system is described and the main parameters of the structure are computed. In §3, a numerical model representing the actual system is developed, and in §4 experimental tests on the linear and nonlinear configuration of the system aimed at tuning the model parameters and validating the model are presented. Finally, in §5 partial feedback linearisation of the system is performed both numerically and experimentally.

2 THE THREE DEGREE-OF-FREEDOM NON-SMOOTH NONLINEAR SYSTEM

The aim is to design a simple system with a non-smooth nonlinear spring, with the facility to alter its nonlinear characteristics as desired. The nonlinear spring is designed to behave in a piece-wise linear manner, and to allow adjustment of the nonlinearity parameters with relative ease.

Figure 1 – Three-degree-of-freedom nonlinear system: design(left),manufactured(right).

The approach is to linearise the system with a force provided by an electromagnetic shaker, such that a control law derived on the basis of feedback linearisation theory is implemented. The system should satisfy two main requirements: (i) it should not be excessively stiff, so that the magnitude of force required for the linearisation can be achieved with the available hardware, and (ii) the effect of the nonlinearity should be evident in the range of displacements covered by the stroke of the shaker. The concept is a simple test rig consisting of three masses and a plate-spring linking them. The designed system is presented in Fig. 1. The nonlinear spring is located in the first mass, but can be easily moved to the second or the third mass. The parameters describing the nonlinearity in the spring are g_1, g_2, defining the point at which the stiffness changes, and $\beta, \alpha_1, \alpha_2$, defining the magnitude of stiffness in each of the two stiffness regions (Fig. 2). The following parameters result: global stiffness k_g for the two springs in parallel fixed to the ground, stiffness $k_{1,2}, k_{2,3}$ for the relative springs that couple the different masses, and the additional setting spring that introduces nonlinear behaviour. With this nonlinear system design, the parameter β is fixed, as it is determined by the stiffness of the grounded spring and therefore cannot be adjusted. All the other parameters are adjustable: the gaps g_1 and g_2 can be regulated by screwing or unscrewing the nuts at the base of the additional spring to reduce or increase the gap between the additional spring and the grounded spring. The parameters related to the external stiffness characteristic α_1 and α_2 can be adjusted by changing the vertical position of the slider. The non-smooth nonlinear spring characteristic can be adjusted symmetrically (but not necessarily) for both gaps and stiffness values.

Furthermore, it is possible to adjust the stiffness of the coupled springs by changing the vertical position of the rigid link which characterises them. The system can be studied as a discrete mass-spring-damper system with all the main mass concentrated in the three masses - considered rigid - and the stiffness concentrated in the plate, assumed to have negligible mass.

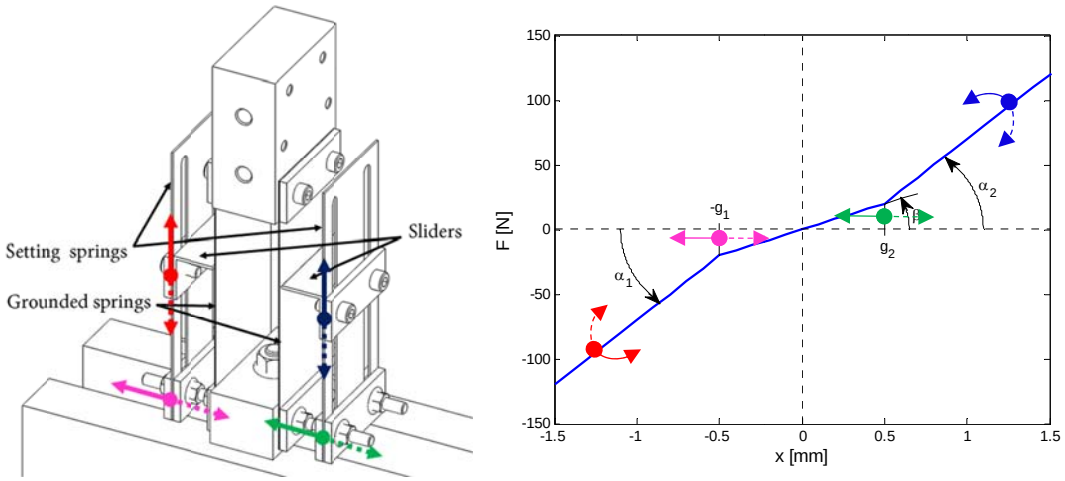

Figure 2 - Non linear spring model (left), spring characteristic (right) and regulation.

The spring stiffness values are evaluated using classical Euler-Bernoulli beam theory, which is appropriate due to the thin aspect ratio of the rectangular cross-sections. The stiffness k_1 of the grounded beam (Fig. 3a) can be computed by considering the beam as being fixed at the root, and having lateral translations at the end. As there are two such beams, the total grounded linear spring stiffness k_g is $2k_1$. When the grounded spring is in contact with the slider of the setting spring, the stiffness changes abruptly. To study the stiffness of the system "one grounded spring plus setting spring", both for the left and right parts of the spring characteristic, it may be observed that the stiffness $k_2(l_2)$ of this system increases when the vertical position of the slider is increased. This spring configuration can be interpreted as a single beam consisting of two segments having different cross-sections (Fig. 3b): the lower segment (between the root and the slider) with an equivalent section given by the sum of grounded and setting springs and the upper segment with equivalent section equal to the grounded beam section.

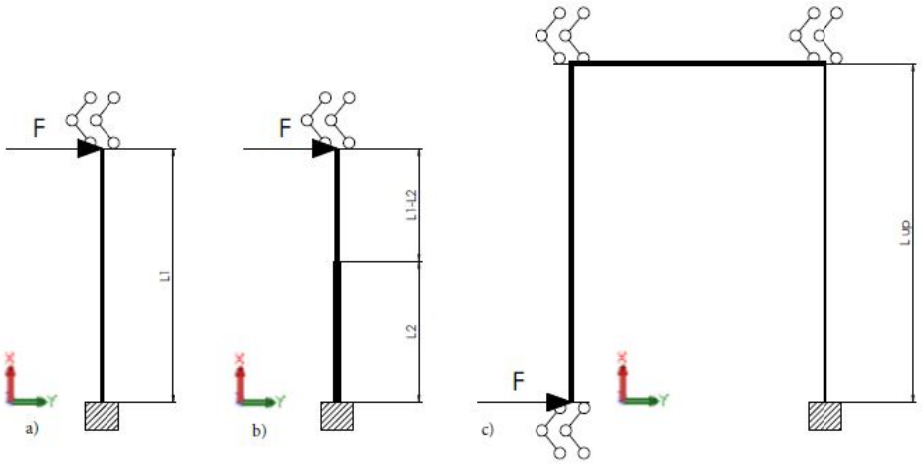

Figure 3 – Model of springs: a) Grounded, b) Grounded plus settin „ c) Coupled.

The complete definition of the nonlinear spring stiffness is:

$$k_{g,nl} = \begin{cases} k_1 + k_2 \\ 2k_1 \\ k_1 + k_2 \end{cases} = \begin{cases} k_g/2 + k_2 & x \le -g_1 \\ k_g & -g_1 \le x \le g_2 \\ k_g/2 + k_2 & x \ge g_2 \end{cases}. \quad (1)$$

The nonlinear spring characteristic changes as a function of the length l_2, as shown in Fig. 4.

The coupled spring is modelled as two bending springs and a rigid link (Fig. 3c); the constraints are the same as in the grounded spring. The coupled spring is designed such that one may change its stiffness $k_{i,i+1}(l_{up})$, by changing the position of the rigid link, and thereby the length l_{up}. Thus, the stiffness of the coupled spring is inversely proportional to the cube of the length. The mass of each degree of freedom has been computed by summing the mass of the block mass at that degree of freedom, the mass of the grounded spring and half the mass of the coupled spring, for each side of the mass linked to another mass. The stiffness and mass parameters are summarised in Table 1.

Table 1: System lumped parameters.

Parameter
k_1=1808.7 N/m
k_g=3616.4 N/m
$k_{2,\min} = k_2(l_2 = 0)$=1808.7 N/m
$k_{2,\max} = k_2(l_2 = l_1)$=10036.6 N/m
$k_{i,i+1}(l_{up} = l_{up,\max})$=1735.5 N/m
m_1=1.456 kg
m_2=2.440 kg
m_3=1.219 kg

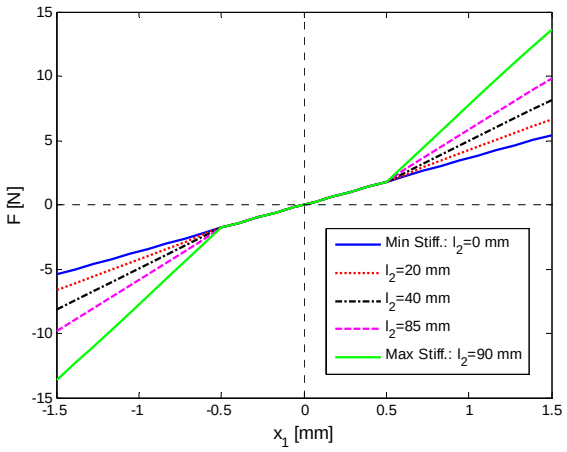

Figure 4 - Nonlinear spring characteristic.

3 MATHEMATICAL MODEL

The system represented in Fig. 1 is a 3 degree-of-freedom discrete system. The nonlinear spring is located in the first mass. Although the aim is to introduce nonlinear behaviour in the stiffness, one also introduces some nonlinear damping due to friction and impact between the slider and grounded spring.

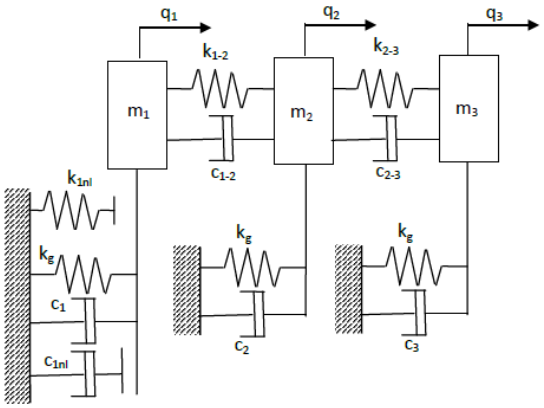

Figure 5 - Sketch of the 3 degrees-of-freedom nonlinear system.

The equation of motion of the system, in the time domain is:

$$\mathrm{M}\ddot{\mathrm{q}} + \mathrm{C}\dot{\mathrm{q}} + \mathrm{K}\,\mathrm{q} + \mathrm{f}_{\mathrm{knl}} + \mathrm{f}_{\mathrm{cnl}} = \mathrm{f}(t). \qquad (2)$$

where q contains the displacements associated with the three degrees of freedom, M,C,K are the mass, damping and stiffness matrices respectively, $\mathrm{f}_{\mathrm{knl}}$ is the vector of forces due to the nonlinear stiffness, $\mathrm{f}_{\mathrm{cnl}}$ is the vector of forces due to nonlinear damping and $\mathrm{f}(t)$ is the excitation applied to the system. The structure and parameters pertaining to the above quantities are expressed as

$$\mathrm{q}=\begin{Bmatrix} q_1 \\ q_2 \\ q_3 \end{Bmatrix} \Rightarrow \dot{\mathrm{q}}=\begin{Bmatrix} \dot{q}_1 \\ \dot{q}_2 \\ \dot{q}_3 \end{Bmatrix} \Rightarrow \ddot{\mathrm{q}}=\begin{Bmatrix} \ddot{q}_1 \\ \ddot{q}_2 \\ \ddot{q}_3 \end{Bmatrix}, \quad \mathrm{M}=\begin{bmatrix} m_1 & 0 & 0 \\ 0 & m_2 & 0 \\ 0 & 0 & m_3 \end{bmatrix},$$

$$\mathrm{K}=\begin{bmatrix} k_g+k_{12} & -k_{12} & 0 \\ -k_{12} & k_g+k_{12}+k_{23} & -k_{23} \\ 0 & -k_{23} & k_g+k_{23} \end{bmatrix}, \quad \mathrm{C}=\alpha\,\mathrm{M}+\beta\,\mathrm{K}, \quad \mathrm{f}(t)=\mathrm{G}\,f(t)=\begin{Bmatrix} 1 \\ 0 \\ 0 \end{Bmatrix} f(t) \qquad (3)$$

The nonlinear forces may be expressed as:

$$\mathrm{f}_{\mathrm{knl}}=\begin{cases} \mathrm{K}_{\mathrm{nl}}\left(\mathrm{q}-\left\{-g_{p_1},0,0\right\}^T\right) & \text{if } q_1<-g_{p_1} \\ 0 & \text{if } -g_{p_1}\le q_1\le g_{p_2} \\ \mathrm{K}_{\mathrm{nl}}\left(\mathrm{q}-\left\{+g_{p_2},0,0\right\}^T\right) & \text{if } q_1>g_{p_2} \end{cases}, \quad \mathrm{K}_{\mathrm{nl}}=\begin{bmatrix} -\frac{k_g}{2}+k_2 & 0 & 0 \\ 0 & 0 & 0 \\ 0 & 0 & 0 \end{bmatrix} \qquad (4)$$

$$\mathrm{f}_{\mathrm{cnl}}=\begin{cases} \mathrm{C}_{\mathrm{nl}}\dot{\mathrm{q}} & \text{if } q_1<-g_{p_1} \\ 0 & \text{if } -g_{p_1}\le q_1\le g_{p_2} \\ \mathrm{C}_{\mathrm{nl}}\dot{\mathrm{q}} & \text{if } q_1>g_{p_2} \end{cases}, \quad \mathrm{C}_{\mathrm{nl}}=\alpha\begin{bmatrix} \mathrm{M}(1,1) & 0 & 0 \\ 0 & 0 & 0 \\ 0 & 0 & 0 \end{bmatrix}+\beta\begin{bmatrix} \mathrm{K}(1,1) & 0 & 0 \\ 0 & 0 & 0 \\ 0 & 0 & 0 \end{bmatrix} \qquad (5)$$

From a comparison between experimental and numerical results for the linear system (Table 3) it is evident that β is many orders of magnitude smaller than α, thus its influence is negligible. The quantity of energy lost depends on the force: the higher the force, the higher the impact, hence the higher the energy lost due to friction, and the energy moved to a higher vibration mode associated with the setting springs:

$$\alpha=\alpha(\mathrm{f}(t))=\gamma\cdot(f(t)), \qquad (6)$$

where γ is a constant coefficient. Thus, it is possible to define:

$$\mathrm{C}_{\mathrm{nl}}(1,1)=\gamma\ \mathrm{M}(1,1)\cdot(f(t))=\Gamma\cdot(f(t)), \qquad \Gamma=\gamma\ \mathrm{M}(1,1), \qquad (7)$$

All model parameters may be calculated beforehand, or are directly measurable, except for α, β and γ which are experimentally evaluated.

4 EXPERIMENTAL TEST

Two different types of experimental tests have been performed on the system to validate the numerical model and to tune the parameters to take into account the manufacturing tolerances that influence both the stiffness of the springs and mass of each degree of freedom. The nonlinear three-degree-of-freedom system can be made linear, by removing the nonlinear spring. For the linear system, an impact test has been adopted, while stepped-sine testing has been used for the nonlinear system.

4.1 Impact test: experimental results and comparison with numerical model

Modal analysis was used to characterise the linear system dynamics. The mass 1 was excited with an impact hammer and the response of the structure was measured with accelerometers. Natural frequencies and damping ratios of the first 3 modes were then identified (Table 2).

The experimental results obtained from the impact tests on the linear system were used to tune the linear parameters and to evaluate the damping of the system. The proportional viscous damping coefficients α and β were computed from the experimental damping ratios and natural frequencies, through a least-square approach on the damping ratios (Table 3).

Table 2: Mean values of natural frequencies and damping ratios.

Mode	f_r [Hz]	ζ_r [%]
1	6.97	0.1524
2	9.66	0.1793
3	10.98	0.1753

The numerical values of the masses were measured; the errors are most likely related to the equivalent mass of the grounded and coupled springs and how these masses are distributed between each degree of freedom. The physical mass was extracted through an inverse modal mass approach from experimental modes shapes and modal masses (Table 4).

Discrepancies between actual and computed stiffness values may arise due to factors such as the actual Young modulus value being different from that assumed, differences between assumed and real thickness and length of each spring, neglecting the influence of the assembly of the coupled spring etc. The tuning of the springs' stiffness values has been achieved by minimising the error between mean experimental natural frequency and model natural frequency, by adjusting three different gains for each stiffness (Table 5).

Table 3: Proportionality viscous damping coefficients.

Coefficient
α =0.058 [rad/s]
β =4.04·10^{-5} [s/rad]

Table 4: Physical mass values

Dof	Meas. - Estim. [kg]
1	1.456 - 1.318
2	2.440 - 2.431
3	1.219 - 1.223

Table 5: Optimal stiffness gains.

Gain
g_1 =0.960
g_2 =0.684
g_3 =0.976

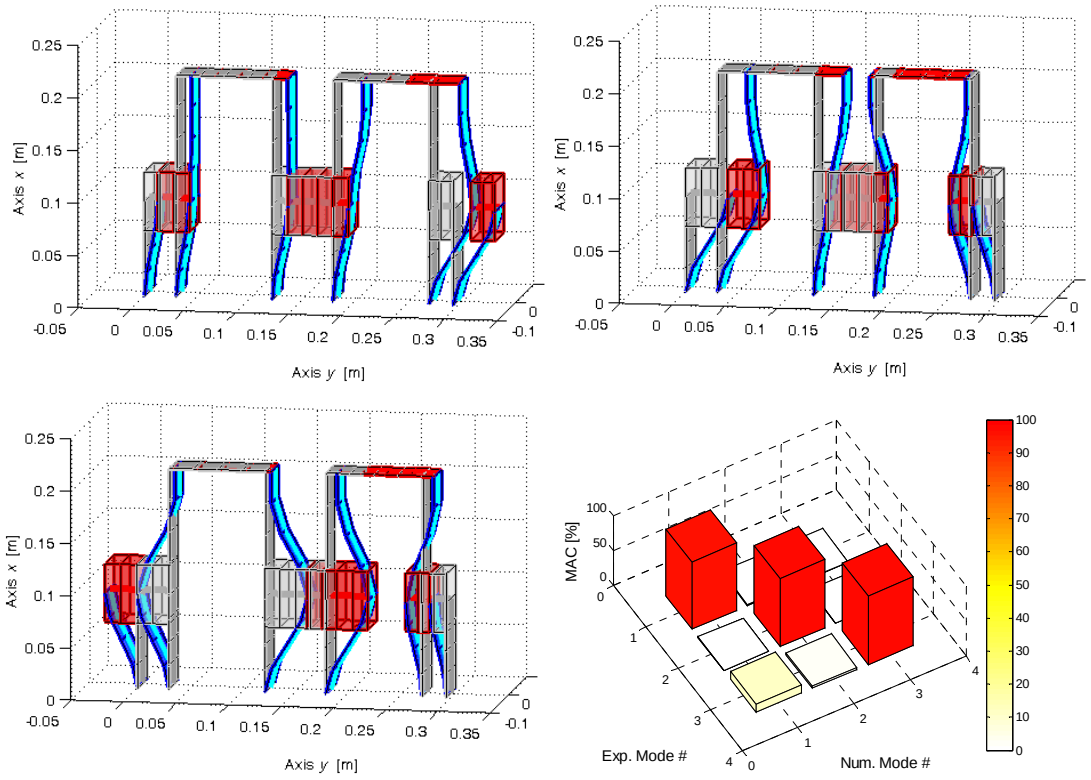

Figure 6 - Mode shapes: Mode 1 – 6.976 Hz (above, left), Mode 2 – 9.664 Hz (above, rigtht), Mode 3 – 10.982 Hz (bottom, left) , MAC between exp. and num. mode shapes(bottom, right).

$$\tilde{k}_g = g_1 k_g,\ \tilde{k}_{1-2} = g_2 k_{1-2},\ \tilde{k}_{2-3} = g_3 k_{2-3}. \quad (8)$$

The values of the gains are very close to 1, except g_2 probably due to differences related to the assembly of the springs, the thickness of the plates and the residual stress due to the slots'

manufacturing process. They are all less than 1, which is expected, as it is unlikely that the actual supports ensure perfect clamped conditions, as assumed in the analysis.

The numerical linear model is obtained from the nonlinear one, by suppressing all the nonlinear terms:

$$\mathrm{M}\,\ddot{\mathrm{q}} + \mathrm{C}\,\dot{\mathrm{q}} + \mathrm{K}\,\mathrm{q} = \mathrm{f}(t). \tag{9}$$

The equation of motion, in state space for is then:

$$\dot{\mathrm{x}} = \mathrm{A}_l \mathrm{x} + \mathrm{B}_l f(t),\ \ \mathrm{A}_l = \begin{bmatrix} 0 & \mathrm{I} \\ -\mathrm{M}^{-1}\mathrm{K} & -\mathrm{M}^{-1}\mathrm{C} \end{bmatrix},\ \mathrm{B}_l = \begin{Bmatrix} 0 & 0 & 0 & \left(\mathrm{M}^{-1}\mathrm{G}\right)^T \end{Bmatrix}^T \tag{10}$$

The mode shapes of the linear system are reported in Fig. 6; the comparison between experimental and numerical mode shapes is done through the Modal Assurance Criterion (MAC).

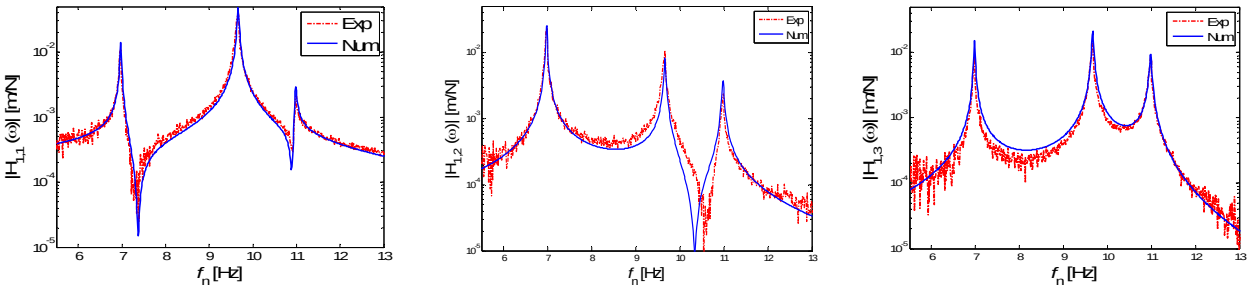

Figure 7 – Comparison of numerical and experimental receptances: $\alpha_{1,1}$ (left), $\alpha_{1,2}$ (middle) and $\alpha_{1,3}$ (right).

The frequency domain content is described from the FRFs of the system (Fig. 7). It can be seen that the numerical model matches very well the natural frequencies of the three-degree-of-freedom system. The errors are less than 1 % for all the natural frequencies of the system; also the damping ratios are in good agreement.

4.2 Stepped-sine tests: experimental results and comparison with numerical model

In order to verify the nonlinear behaviour of the system, and to tune the empirical nonlinear damping coefficient γ, several stepped-sine tests were performed between the frequency range 5 Hz - 35 Hz. The parameters of the nonlinear spring – which is located in the first mass – are: k_2 = 7450 N/m and $g_1 = g_2$ = 0.4025 mm.

The excitation force amplitude is maintained almost constant for each test, and a different amplitude was used for each test. The step size used was 0.1 Hz for all the four tests.

In the experimental results (Fig. 8) the first and the third peaks are not affected significantly by the nonlinearity; instead a nonlinear peak appears in the second mode range, associated with the first mass, where the nonlinear hardening spring is located. From FRF 1,1 (Fig. 8, left), it is very clear that the amplitude of the mode reduces as the excitation force amplitude is increased.

The numerical nonlinear FRFs are obtained from the envelope of the time domain response of the system, excited with a sine-sweep in which the excitation frequency $\Omega(t)$ varies linearly with time, but slowly compared to the natural periods of the system [16]. The constant coefficient γ, identifying the nonlinear damping, has been tuned to have the jump at the right frequency, according to the experimental results; the value of γ satisfying the entire excitation level is γ = 17.5 rad s^{-1} N^{-1}.

The minor differences between numerical and experimental results are attributable to the fact that the amplitude of the experimental force, although intended, is not exactly constant, for different values of frequency and between different tests. The comparison between experimental and

numerical results confirms that the mathematical model is sufficiently accurate to describe the system's nonlinear behaviour.

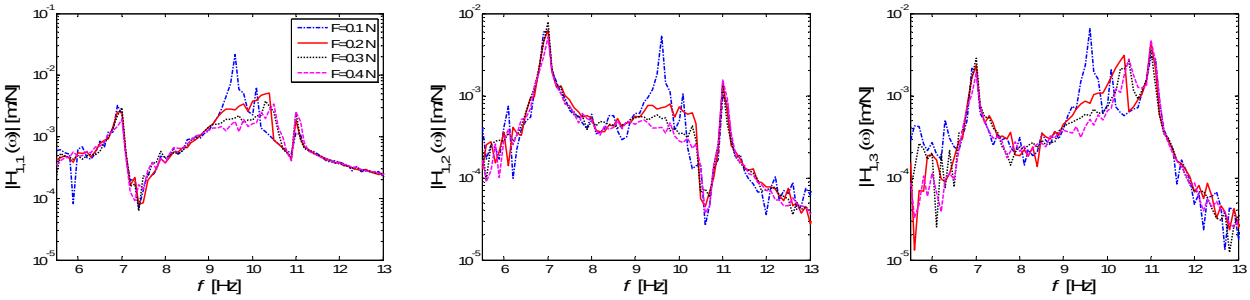

Figure 8 - Experimental nonlinear FRF, with changing force amplitude: FRF 1,1.(left), FRF 1,2 (middle), FRF 1,3 (right).

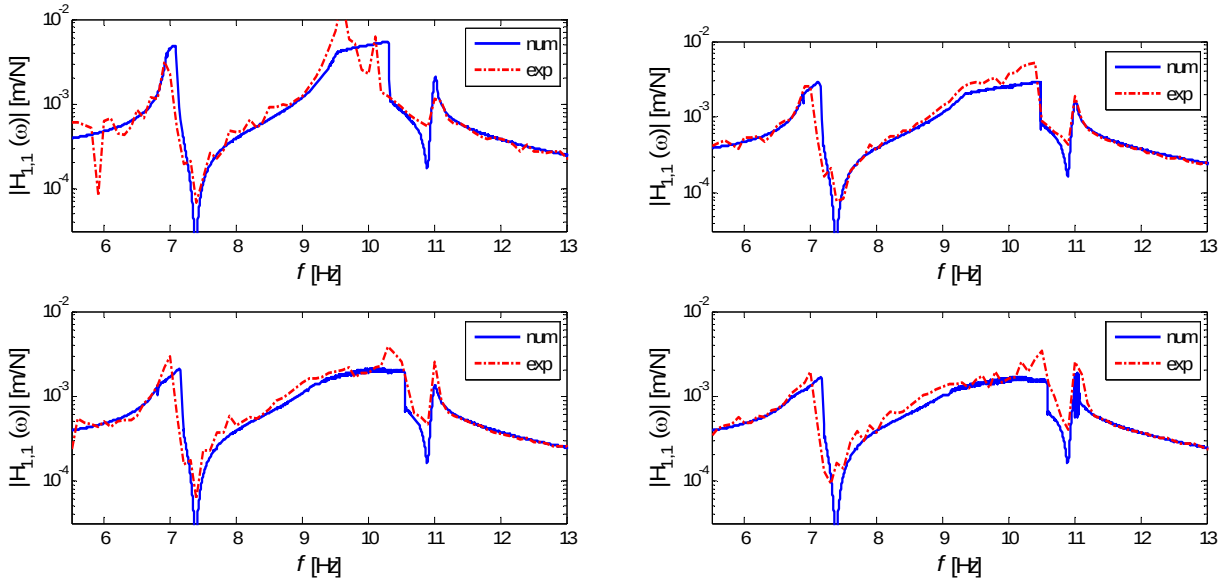

Figure 9 – Experimental vs. numerical FRF 1,1, with changing force amplitude: F = 0.1 N (above, left), F = 0.2 N (above, right), F = 0.3 N (bottom, left) and F = 0.4 N (bottom, right).

5 PARTIAL FEEDBACK LINEARISATION

The aim of partial feedback linearisation is to linearise certain chosen modes of the system by replacing its nonlinear dynamics with linear dynamics. In the present case, input-output feedback linearisation is implemented, which uses a virtual input and a coordinate transformation to linearise the nonlinear system often described as [1-3]:

$$\dot{\mathrm{x}} = \underline{\mathrm{f}}(\mathrm{x}) + \underline{\mathrm{g}}(\mathrm{x})u(t), \quad u(t) = \varphi(\mathrm{x}) + \rho(\mathrm{x})\bar{u}(t), \quad \mathrm{z} = \mathrm{T}(\mathrm{x}), \tag{11}$$

where $u(t)$ is the real input to the nonlinear system, $\bar{u}(t)$ is a "virtual input" corresponding to the linearised system, z is the linearised state vector and the matrix T allows transformation between linear and nonlinear co-ordinates.

The equation of motion of the three degree of freedom system, Eq. (2), can be rearranged in the above form. The displacement associated with the first degree of freedom is chosen as the output y, for the input-output linearisation procedure; this is the degree of freedom where the non-smooth nonlinearity is located. The complete set of equations representing the partially linearised system is obtained by combining with the output equation its n time-derivatives. n is the relative degree of the single input single output (SISO) system, i.e. the number of times it is necessary to differentiate the output before the input term explicitly contributes to the linearised dynamics. For

the present system input-output linearisation, it can be shown that the relative degree of the system is n=1, therefore the linearisation is partial because n is less than the dimension of the state vector x. Following the procedure for input-output linearisation, it can be shown that the system, in linear coordinates can be expressed as [17]:

$$\begin{Bmatrix} \dot{z}_1 \\ \dot{z}_2 \end{Bmatrix} = \begin{bmatrix} 0 & 1 \\ 0 & 0 \end{bmatrix} \begin{Bmatrix} z_1 \\ z_2 \end{Bmatrix} + \begin{Bmatrix} 0 \\ 1 \end{Bmatrix} v, \tag{12}$$

where v is the artificial input, which can be chosen to specify the dynamics of the linearised system. For example, the pole-placement law $v = -\omega_n{}^2 z_1 - 2\zeta_n \omega_n z_2$ assigns natural frequency ω_n and damping ratio ζ_n to the linearised system.

5.1 Internal dynamics

It is not possible to control the entire dynamics of the new system, as the full system has dimension 6 while the linearised system only has dimension 2. Thus, there remains an un-linearised portion of dimension 4, known as the internal dynamics. The full transformation matrix T, where $\mathrm{z} = \mathrm{T}\,\mathrm{x}$, can be chosen arbitrarily provided that (a) it is non-singular and (b) the dynamics associated with the additional co-ordinates are orthogonal to $\mathrm{g}(\mathrm{x})$. The latter condition ensures that the internal dynamics are obtained in the normal form, where the system inputs do not appear. The stability of the internal dynamics is necessary to ensure overall stability of the closed-loop system. This can be verified by studying the stability of the zero-dynamics, found by setting to zero the coordinates corresponding to the linearised state variables in the internal dynamics. For the present system, the zero dynamics are found to be:

$$\dot{\mathrm{z}}_{zd} = \begin{Bmatrix} \dot{z}_3 \\ \dot{z}_4 \\ \dot{z}_5 \\ \dot{z}_6 \end{Bmatrix} = \begin{Bmatrix} z_5 \\ z_6 \\ -(1/m_2)\left[\left(k_g + k_{12} + k_{23}\right) z_3 - k_{23} z_4 + c_{2,2} z_5 + c_{2,3} z_6\right] \\ -(1/m_3)\left[-k_{23} z_3 + \left(k_{23} + k_g\right) z_4 + c_{3,2} z_5 + c_{3,3} z_6\right] \end{Bmatrix}. \tag{13}$$

By simulating Eq. (13) with an initial perturbation, it is found that all variables in the zero dynamics decay to zero, which indicates that the internal dynamics are stable.

5.2 Closed loop simulation and effects of uncertainties

Feedback linearisation is a method that requires a numerical model, which is the basis for the synthesis of the linearising control law. Thus, the more representative the model is of the physical system, the more accurate the results. In the numerical model, the parameters representing the system dynamics are exactly equal to the parameters assumed in the control law, therefore the linearisation is ideal. A closed loop simulation has been performed on the nonlinear system to demonstrate the effect of the active control. A representative result is reported in Fig. 10.

The response is in open loop for the first 2 seconds, during which time the time domain response is nonlinear and the frequency of oscillation is the natural frequency of the first mode. At the instant t = 2 s, the controller is activated and the response is linearised. In this way the linearised degree of freedom behaves like a single degree of freedom system, completely uncoupled from the other two degrees of freedom, and it vibrates with the assigned natural frequency and damping ratio.

In simulation, the linearisation is perfect for reasons explained above. In the real case, however, it is impossible to achieve perfect partial feedback linearisation because of errors between the assumed and actual parameters of the system. Small errors in the mass, stiffness and damping values of the system can produce an inexact cancellation of the dynamics of the system, and therefore in the experimental results more than one single harmonic can be present. The system is a non-smooth nonlinear system, therefore the nonlinear parameters are particularly influential on the

closed loop response. In particular, the system is very sensitive to the gaps between the sliders and grounded springs. The gaps are very small, therefore it is difficult to measure it with high accuracy.

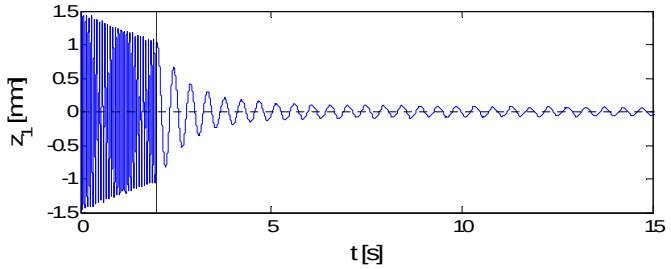

Figure 10 – Closed loop response, pole placement parameters: $f_n = 2$ *Hz,* $\xi = 0.1$

The control law requires the gaps magnitudes, and so the dynamics of the closed-loop system will be affected if the model gaps are different from the real one. It is possible to study what happens in this situation in a numerical simulation, by modelling errors between the real gaps $g_{1,2}$ included in the system dynamics model and the measured gaps $g_{m1,2}$ specified in the control law. Two case are analysed, assuming a symmetric piecewise characteristic: (i) $|g_{m1,2}| > |g_{1,2}|$,(ii) $|g_{m1,2}| < |g_{1,2}|$. In both cases the pole placement parameters are f_n = 5 Hz and ξ = 0.1. In the first case the assumed parameters are $g_{1,2}$ = 0.5 mm and $g_{m1,2}$ = 0.55 mm, whereas in the second case $g_{1,2}$ = 0.5 mm and $g_{m1,2}$ = 0.2 mm. The simulation results of the two cases are reported in Fig. 11 and Fig. 12 respectively. It is evident that the system linearisation is highly influenced by the gaps: when the measured gaps are greater than the real ones a limit cycle is established and the response never decays to zero, whereas when the measured gaps are smaller than the real ones, the system goes to a stable position in much less time than in the ideal case, but the stable point is non-zero.

In these conditions the input deletes exactly the linear part of the system dynamics, whereas the nonlinear dynamics are not entirely eliminated. Considering Fig. 11, in the time period between $x_1(t_1) = |g_{1,2}|$ and $x_1(t_2) = |g_{m1,2}|$ there is no force input, although there should be, therefore the nonlinearity is not completely eliminated and a limit cycle is established.

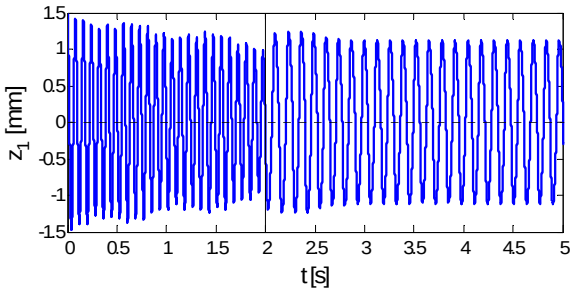

Figure 11 - Closed loop response, $|g_{m1,2}| > |g_{1,2}|$

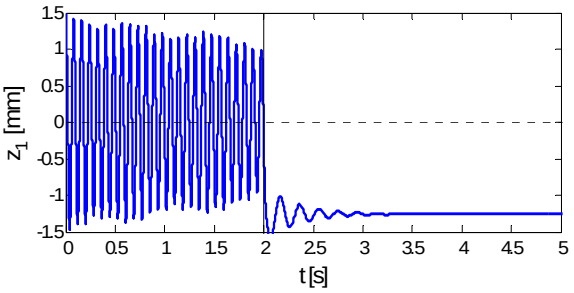

Figure 12 - Closed loop response, $|g_{m1,2}| < |g_{1,2}|$.

In Fig. 12, instead, there is a displacement range in which the nonlinearity is not eliminated, so a static non-zero displacement is established; this condition introduces a free-play nonlinearity in the already piecewise nonlinear spring characteristic [15]. Knowing the behaviour of the system in these two conditions is useful to tuning the model gaps in the experimental test.

5.3 Experimental partial feedback linearisation

The three degree-of-freedom non-smooth nonlinear system is partially linearised experimentally. The experimental tests on the non-smooth nonlinear system are useful to evaluate the ability of the control law to partially linearise the system and thereby introduce the desired dynamics.

The closed loop response should cancel out all the nonlinearities of the system, and also the linear part of the system dynamics; it should replace the dynamics with the specified natural frequency and damping ratio in the linearised degree of freedom, through a pole placement control law. In simulation it is simple to obtain these results, as it is possible to assign whatever natural frequency and damping ratio that is desired. In the experimental case, however, it is very difficult to change the natural frequency of the system, as it is impossible to cancel out entirely the dynamics of the system, although it is possible to define a damping ratio, with reasonable success. The experimental test has been performed using an assigned natural frequency quite close to the open-loop oscillation frequency, and trying to change the damping ratio of the modes associated with the linearised states. The experimental partial feedback linearisation test has to be performed in real time, because the input force depends on the instantaneous displacements and velocities of the three masses.

Figure 13 - Experimental partial feedback linearisation setup.

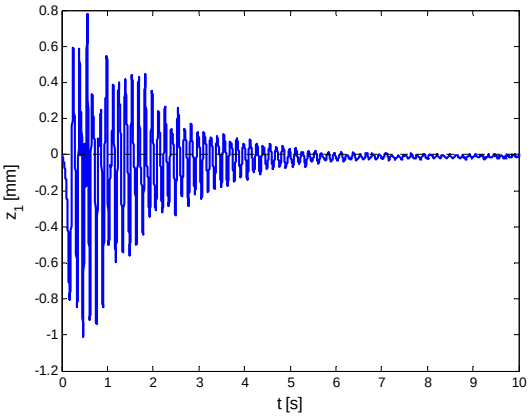

Figure 14 - Closed loop response: $f_n = 7\ Hz, \zeta = 0.03$.

Three laser displacement sensors were used to measure the displacements, one for each mass. An electromechanical shaker was used as the actuator, and a load cell provided the value of force applied to the system. The signals from the laser sensors were processed by dSPACE® hardware and the software developed within ControlDesk®.

The experimental setup is shown in Fig. 13. The control tests were performed by perturbing the system without attention to the initial conditions, because assigning the same initial conditions for each test proved difficult. In the tests the damping ratio was varied between $\zeta = 0.01 \div 0.1$, with a step size of 0.01.

Table 6: Assigned and measured damping ratio.

	ζ	ζ_{exp}	**Err. [%]**
1	0.01	0.0107	+6.88
2	0.02	0.0217	+8.80
3	0.03	0.0272	-9.18
4	0.04	0.0455	13.80
5	0.05	0.0897	+79.53
6	0.06	0.0443	-26.08
7	0.07	0.0637	-8.95
8	0.08	0.0625	-21.76
9	0.09	0.0800	-11.02
10	0.1	0.0746	-25.39

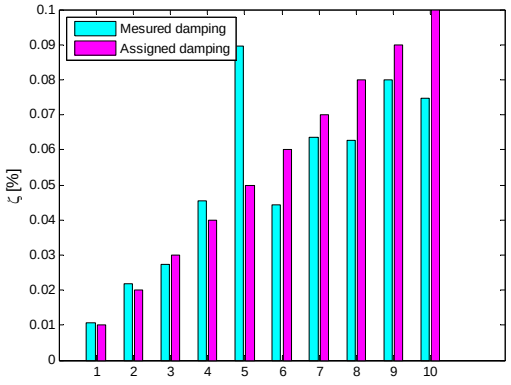

Figure 15 – Comparison between assigned and measured damping ratio.

One of the recorded system responses is reported in Figure 14. The real damping ratio was extracted from the time domain responses and compared with the assigned one, to verify that damping of the closed loop system was indeed close to the assigned one. The method of the logarithmic decrement was used to extract the damping ratio from the recorded time domain

responses. This method is valid for linear single degree of freedom systems. The partially linearised system should be linear and the first mass, after the linearization, should be a single degree of freedom system uncoupled from the remainder of the non-smooth nonlinear system. Thus, the theoretical conditions for applying logarithmic decrement were satisfied. The results are reported in Table. 6 and Fig. 15. The extracted damping ratio of the linearised system increases, following closely the assigned value. For lower values, the measured damping is very near to the assigned one, whereas for higher values the damping increases, but is not as close to the assigned one. The comparison is good for all time domain responses recorded, except in the case of $\zeta = 0.05$. This is not particularly problematic, as errors in the range of 50 % are not uncommon when comparing experimental and numerical values of damping.

6 CONCLUSION

In this paper, the authors have presented results from the experimental application of feedback linearisation to a non-smooth nonlinear system. A test rig comprising a non-smooth nonlinearity in stiffness has been designed and manufactured, and a representative numerical model has been created for simulation purposes and also synthesis of the controller. After tuning the system parameters in the numerical model, the validity of the model has been ascertained from the close agreement between numerical and experimental results. The experimentally measured frequency response function of the linear system is reproduced with good accuracy in the numerical simulation; this is also true in the nonlinear case, which indicates that the modelling of the nonlinear stiffness and damping is accurate. The application of feedback linearisation on this non-smooth nonlinear system has been demonstrated in numerical simulations. The results in the closed-loop case are as expected, while in the experimental case good results have been achieved in assigning the damping ratio of the system. The results from this work are an encouraging indication of the applicability of the feedback linearisation method to non-smooth nonlinear systems. The natural future development of this work is the application in simulation and in experiment adaptive feedback linearisation to alleviate problems related mainly to the gap values, but also to other sources of error.

ACKNOWLEDGEMENTS

The authors gratefully acknowledge the support of the Engineering and Physical Sciences Research Council grant EP/J004987/1 on Nonlinear Active Vibration Suppression in Aeroelasticity. The authors would also like to acknowledge fellow researcher Dr. Sebastiano Fichera in the School of Engineering, University of Liverpool, for his support, contributory to the overall outcome of this work.

REFERENCES

[1] Isidori, A., *Nonlinear Control Systems*, Springer, 1995.

[2] Khalil, H.K., *Nonlinear Systems*, Prentice Hall, 2002.

[3] Vidyasagar, M., *Nonlinear system analysis*, Prentice Hall, 1993.

[4] Jiffri, S., Paoletti, P., Cooper, J.E. & Mottershead J.E., Feedback linearisation for nonlinear vibration problems, *Shock and Vibration*, 2014.

[5] Jiffri, S., Mottershead, J.E. & Cooper, J.E., Adaptive Feedback Linearisation and Control of a Flexible Aircraft Wing, *Topics in Modal Analysis*, Volume 7, Proceedings of the 31st IMAC, A Conference on Structural Dynamics, Orange County CA, USA, 2013, pp. 683-699.

[6] Spong, M., Partial feedback linearization of underactuated mechanical systems, Proc. IEEE, Munich, Germany, 1994, pp. 314-321.

[7] Pathak, K., Franch, J. & Agrawal S., Velocity and position control of a wheeled inverted pendulum by partial feedback linearization, *IEEE transactions on robotics*, 2005, **21**(3), pp. 505-513.

[8] Gans, N. & Hutchinson, S., Visual servo velocity and pose control of a wheeled inverted pendulum through partial-feedback linearization, *Proc. IEEE*, Beijing, China, 2006, pp. 3823-3828.

[9] Tuan, L., Lee, S., Dang, V., Moon, S. & Kim, B., Partial feedback linearization control of a three-dimensional overhead crane, *International Journal of Control, Automation, and Systems*, 2013, **11**(4), pp. 718-727.

[10] Tuan, A., Kim, G., Kim, M. & Lee, S., Partial feedback linearization control of overhead cranes with varying cable lengths, *International Journal of Precision Engineering and Manufacturing*, *2012,* **13**(4), pp. 501-507.

[11] Marino, R., Pereseada, S. & Valigi, P., Adaptive partial feedback linearization of induction motors, *Proc. 29th Conference on Decision end Control*, Honolulu, Hawaii, 1990, pp. 3313-3318.

[12] Xiang, F. & Wikander, J., Block-oriented approximate feedback linearization for control of pneumatic actuator system, *Control Engineering Practice*, 2004, **12**, pp. 387-399.

[13] Tao, G. & Kokotovic, P., Adaptive control of systems with unknown non-smooth non-linearities, *International Journal of Adaptive Control and Signal Processing*, *1*997*,* **11**, pp. 81-100.

[14] Sun, Z.D. & Ge, S.S., Nonregular feedback linearization: a nonsmooth approach, *IEEE Transactions on Automatic Control*, 2003, **48**(10), pp. 1772-1776.

[15] Jiffri, J., Paoletti, P. & Mottershead, J.E., Feedback linearisation in systems with non-smooth nonlinearities, *Journal of Guidance, Control and Dynamics*, *2016,* **39**(4), pp. 814-825..

[16] Worden, K. & Tomlinson, G.R., *Nonlinearity in Structural Dynamics*, Institute of Physics Publishing, Bristol, 2001.

[17] Da Ronch, A., Tantaroudas, N.D., Jiffri, S. & Mottershead, J.E., A nonlinear controller for flutter suppression from simulation to wind tunnel testing, *55th AIAA/ASME/ASCE/AHS/ASC Structures, Structural Dynamics, and Materials Conference,* 2014.